ACS OMEGA

http://pubs.acs.org/journal/acsodf

Article

Titanium Dioxide Nanotube Arrays for Cardiovascular Stent Applications

Ita Junkar,* Mukta Kulkarni, Metka Benčina, Janez Kovač, Katjuša Mrak-Poljšak, Katja Lakota, Snežna Sodin-Šemrl, Miran Mozetič, and Aleš Iglič

Cite This: *ACS Omega* 2020, 5, 7280−7289

Read Online

ACCESS | Metrics & More | Article Recommendations

ABSTRACT: Efficient stent implantation among others depends on avoiding the aggregation of platelets in the blood vessels and appropriate proliferation of endothelial cells and controlled proliferation of smooth muscle cells, which reduces the development of pathology, such as neointimal hyperplasia, thrombosis, and restenosis. The current article provides an elegant solution for prevention of platelet and smooth muscle cell adhesion and activation on stent surfaces while obtaining surface conditions to support the growth of human coronary artery endothelial cells. This was achieved by surface nanostructuring and chemical activation of the surface. Specific nanotopographies of titanium were obtained by electrochemical anodization, while appropriate chemical properties were attained by treatment of titanium oxide nanotubes by highly reactive oxygen plasma. Surface properties were studied by scanning electron microscopy, atomic force microscopy, and X-ray photoelectron spectroscopy. Wettability was evaluated by measuring the water contact angle. The influence of nanostructured morphology and plasma modification on in vitro biological response with human coronary artery endothelia and smooth muscle cells as well as whole blood was studied. Our results show that a combination of nanostructuring and plasma modification of the surfaces is an effective way to achieve desired biological responses necessary for implantable materials such as stents.

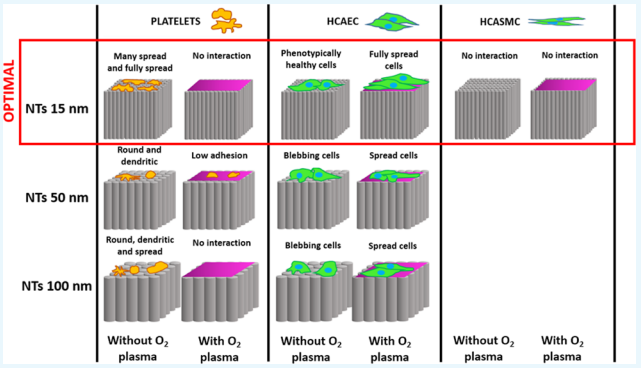

1. INTRODUCTION

Characteristics of titanium and titanium alloys, such as high biocompatibility, corrosion resistance to body fluids, great tensile strength and flexibility have ensured their and extensive use as biomaterials. For more than 50 years, metals have been used in medical applications (orthopedics, dentistry, and vascular surgery).

In cardiovascular applications, stents are commonly employed to enlarge the lumen wall and to restore blood flow through the affected blood vessel. Although titanium alloys are extensively used for stent application, they still lack desired biological responses, mostly due to restenosis and thrombosis. Restenosis still presents a huge problem on all stent surfaces. It occurs in more than 33% of the cases, with higher possibilities in patients with chronic diseases, such as diabetes. Placement of bare metal stent (BMS) in the blood vessel is connected with mechanical injuries of the lumen wall, which initiates a variety of reactions, including platelet activation and thrombus formation, accompanied by inflammation, and proliferation and migration of smooth muscle cells within the media and the intima.[1,2] All these cellular responses lead to thickening of the intima by smooth muscle cells and surrounding extracellular matrix with or without progression to restenosis. Therefore, drug-eluting stents (DES) with various coatings were employed to cut high restenosis rates of BMS. However, problems appeared as these stents highly increased thrombosis with serious consequences as DES inhibited normal growth of endothelium. Therefore, the Food and Drug Administration (FDA) set guidelines for dual antiplatelet therapy up to 12 months after DES implementation.[3] New generation of DES were introduced with more biocompatible polymer coatings. However, dual antiplatelet therapy still could not be eliminated. Therefore, the thrombogenicity and restenosis induction of blood-connecting devices remain a serious concern and should be given a great deal of attention in order to fabricate surfaces with improved tissue-material response.

Received: December 3, 2019
Accepted: March 5, 2020
Published: March 27, 2020

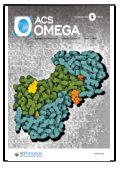

https://dx.doi.org/10.1021/acsomega.9b04118
ACS Omega 2020, 5, 7280−7289

In the literature, we can find many different techniques, which are employed to improve surface properties of stents. Mainly, they are directed at altering and/or coating of stent surfaces in such a manner that the bulk attributes remain unaffected. Procedures and methods for coating stent surfaces are mainly accomplished by silicon carbide, hydroxyapatite, titanium oxides, titanium nitride carbide, plasma thermal sprays, or various polymeric coatings and bioactive coatings like albumin, heparin, chitosan, etc.[4−9] As mentioned above, many drug-eluting coatings are already used in clinical settings; however, the durability and stability of such coatings are still problematic and have been connected with a higher risk for developing thrombosis. Using nanotechnologies in the medical field has directed the designing of nanotopographic features as biomimetic interfaces for implantable devices.[10,11] In vitro results show that surface features on the nanometer scale stimulates and controls several molecular and cellular events on tissue/implant interfaces, which can be observed by differences in cell morphology, orientation, cytoskeleton organization, proliferation, and gene expression,[12,13] among other processes. In the past few years, titanium nanotubes fabricated by various methods, such as sol−gel methods, hydrothermal approaches, and electrochemical anodization, gained significant attention.[14−19] For example, hydrothermal treatment of titanium wires was employed to generate nanotopography that showed negligible hemolysis as well as reduced activation and aggregation of platelets. Moreover, the endothelium formed on the surfaces with nanoscale topography exhibited enhanced expression of antithrombogenic genes, providing for a longer coagulation cascade, probably due to a thicker oxide layer and specific topography.[12] In the past decade, electrochemical anodization was often employed as by this method self-organized titanium dioxide (TiO_2) nanotubes can be formed by facile electrochemical oxidation of titanium substrate.[10,11,16,20−22] By changing the anodization parameters (applied voltage and anodization time), TiO_2 nanotubes of different diameters from 15 to 300 nm of different lengths can be obtained. Excellent potential of titanium nanotubes in medicine and biotechnology is mainly due to its high effective surface and the possibility to vary their geometry (diameter and length), which could be specially designed for a desired biological response. TiO_2 nanotubes have been shown to increase selective protein adsorption[23] and subsequently enhanced biological response. For example, studies showed that TiO_2 nanotubes increase bone growth/regeneration, are antibacterial, and reduce inflammation.[24−27] It was reported by Smith et al. that TiO_2 nanotubes with 70−90 nm diameters actually increase adsorption of blood serum proteins, adhesion and activation of platelets and whole blood clotting kinetics.[28] On the other hand, Yang et al. showed that superhydrophilic and superhydrophobic TiO_2 nanotubes reduce platelet adhesion and activation compared to smooth titanium surface. The same group indicated that significantly lower platelet activation was observed on superhydrophobic surfaces due to special nanostructured features and surface modification with low-energy materials.[29]

Kulkarni et al. reported that binding of proteins from human serum onto TiO_2 nanotubes (NTs) of different diameters, such as serum amyloid A (SAA), a major acute phase protein (known to be elevated up to 1000-fold following infections or tissue injury), was dose-dependent, yielding increased concentrations of SAA bound to larger diameter NTs. This could have implications not only for processes such as inflammation and tissue regeneration but also on antimicrobial properties of the NTs.[15] SAA has also been reported to dose-dependently elevate the levels of released pro-inflammatory interleukin-6 (IL-6) from human coronary artery endothelial cells (HCAEC), which could account for greater susceptibility of HCAEC to inflammation and atherogenesis.[30]

Recently, we studied the performance of HCAEC and human coronary artery smooth muscle cells (HCASMC) on NT surfaces of different diameters in regard to cell proliferation and released IL-6 levels. Previously, we showed that HCAEC activity is dependent on the diameter of the TiO_2 NTs, growing far less optimally when bound to 100 nm TiO_2 NTs, as compared to Ti foil, 15 nm NTs, or 50 nm NTs.[30] They showed improved morphological cell shape changes when grown on oxygen-rich plasma-treated versus non-treated 100 nm NTs. In this report, our aim was to show divergent modes of activation (in terms of adhesion and proliferation) of HCAEC and HCASMC when bound to plasma-treated and non-treated NTs.

The improved biocompatibility of TiO_2 is believed to be attributed to its surface energy and n-type semiconductor properties.[31] Most titanium oxide coatings have been deposited on the surface of the bulk material in a form of thin film from a secondary source, while a more intriguing way is to form TiO_2 from the existing surface, which eliminates concerns regarding coating instabilities. Such approaches are oxygen plasma immersion ion implementation and non-thermal low or atmospheric pressure plasma treatments, which were already shown to increase the oxide layer on titanium materials.[31,32] Thus, the aim of the current work was to study the combined influence of nanotopography and surface chemistry on in vitro biological responses of titanium dioxide. For the purpose of this study, different nanotube morphologies were produced by electrochemical anodization and surface treatment with highly reactive oxygen species being used to alter surface chemistry (oxygen-enriched surface layer and removal of impurities induced by the anodization process). The influence of different nanotube morphologies and surface modification was studied in terms of surface properties, such as wettability, morphology, and chemistry, while in vitro studies were performed, such as endothelial cell proliferation, platelet adhesion, and activation. Interestingly, by optimizing nanotopographic features and chemical composition of the surface, reduced platelet adhesion and activation on TiO_2 nanotubes were achieved. Moreover, plasma-modified TiO_2 surfaces showed improved proliferation of HCAEC. These findings provide valuable information for development of novel types of stent surfaces, which reduce thrombogenic and restenotic complications while, at the same time, providing optimal support for growth of the endothelium.

2. RESULTS AND DISCUSSION

2.1. Nanoscale Morphology of TiO_2 NTs. The morphology of the obtained TiO_2 NTs was evaluated by scanning electron microscopy (SEM) and atomic force microscopy (AFM). The top-view SEM images (see Figure 1) present the surface of Ti foil and the surface of fabricated NTs with three different diameters (15, 50, and 100 nm). The Ti foil served as a reference material for the in vitro biological experiments, and according to SEM images, no special surface morphology on its surface was observed. However, the SEM images with NTs revealed that NTs are uniformly distributed on the surface and that indeed NTs with 15, 50, and 100 nm in

https://dx.doi.org/10.1021/acsomega.9b04118
ACS Omega 2020, 5, 7280−7289

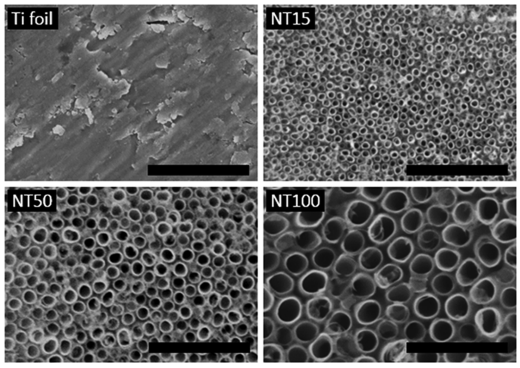

Figure 1. SEM images of the top surface of Ti foil and TiO_2 nanostructures of different diameters: nanotubes with 15 nm (NT15), 50 nm (NT50), and 100 nm (NT100) in diameter; Scale bars: 500 nm.

diameter are formed. Similar observations were found by analysis of surface topography by AFM. The results from AFM enable observations of the 3D nanotube morphology (Figure 2). Differences in nanotopography between the samples were observed as pristine Ti foil was pretty flat with no special topographic features (Figure 2a), while nanostructured features were observed for NT15, NT50, and NT100 (Figure 1). Although the penetration of the AFM tip to nanostructured surfaces was limited, especially for the case of NT15 (Figure 2b), the hollow interior for NT50 and NT100 could be observed (Figure 2c,d). The average surface roughness was measured for all surfaces on a $1 \times 1 \mu m^2$ area. Due to different penetration depths of the AFM tip on different NT diameters, these values give only rough estimations of changes in topography. The results show that pristine Ti foil and NT15 have similar surface roughness, about 11.7 and 10.1 nm, respectively. A slightly higher surface roughness was measured for NT50, about 15.5 nm, and the highest average roughness was measured for NT100, about 25.9 nm. From the 3D images, small variation in the height of the nanotubes can also be observed as, for all samples, a few nanometer differences in the nanotube length is observed from AFM analysis.

2.2. XPS Analysis. Specific diameters of TiO_2 nanotubes were analyzed by XPS. The samples were as follows: Ti foil, freshly prepared NTs (1 week old), old NTs (2 months aged in an ambient atmosphere at 22 °C and relative humidity of 45%), and NTs after treatment with oxygen plasma. In Figure 3, chemical composition of the surface for each sample is

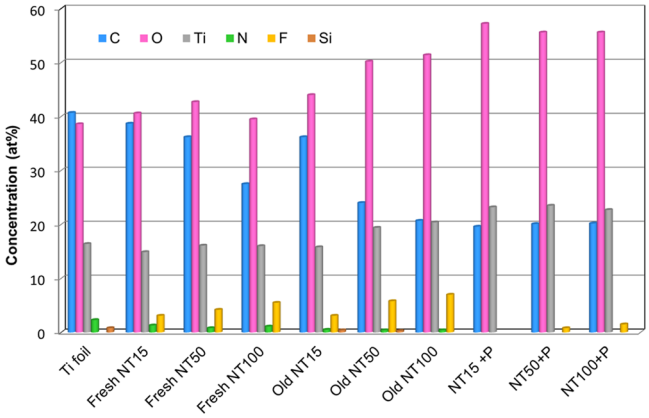

Figure 3. Chemical composition of plain titanium foil (Ti foil) and nanotubes (NTs), which were analyzed by XPS immediately after fabrication (Fresh NT), 1 month after fabrication (Old NT), and after plasma treatment (NT+P).

presented as obtained from the XPS survey spectra. Ti foil has about 41.2 at % of carbon, 38.3 at % of oxygen, and 18 at % of titanium, which is very similar to freshly prepared NTs. The main difference between NTs with different diameters is only in the content of fluorine, which increases with the size of the nanotube diameter. The fluorine content on NTs is observed due to the anodization procedure used for production of NTs. By increasing the size of NTs, less carbon is observed on its surface as it drops from the initial 41.7 at % to about 27.5 at %

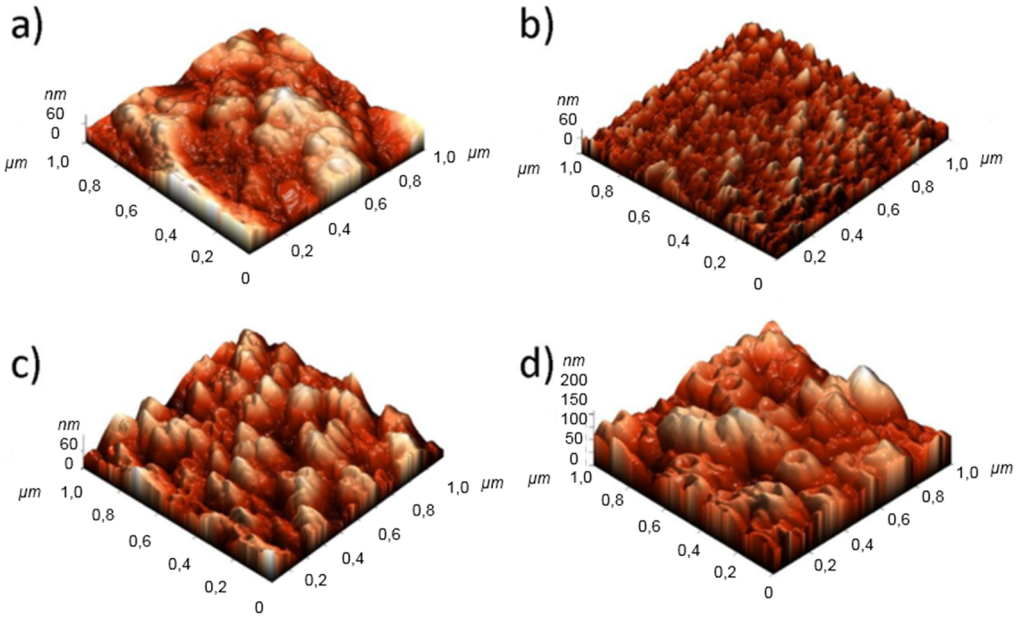

Figure 2. AFM images of pristine Ti foil and TiO_2 nanostructures with different diameters: (a) Ti foil, (b) nanotubes with 15 nm (NT15), (c) 50 nm (NT50), and (d) 100 nm (NT100) in diameter.

https://dx.doi.org/10.1021/acsomega.9b04118
ACS Omega 2020, 5, 7280−7289

Table 1. Results of Water Contact Angle, Chemical Ratio of Ti/O and C/O Obtained from XPS Survey Spectra, and Platelet Adhesion on Plain Titanium Foil, Freshly Prepared NTs, Old NTs, and Plasma Treated NTs with Different Diameters (NT15, NT50, and NT100)

sample	plain Ti foil	fresh NT15	fresh NT50	fresh NT100	old NT15	old NT50	old NT100	NT15+P	NT50+P	NT100+P
WCA (deg)	97.6	<5	<5	<5	117.6	99.7	83.7	<5	<5	<5
XPS (Ti/O)	0.44	0.36	0.38	0.4	0.36	0.38	0.39	0.41	0.42	0.41
XPS (C/O)	0.93	0.95	0.84	0.94	0.82	0.48	0.40	0.34	0.36	0.36
platelet adhesion	very high	high	medium	low	very high	high	high	no	low	no

in the case of NT100. After aging in air, the surface seems to be oxidized, and the oxygen content is increased; thus, an increase from about 40 at % for fresh NT100 to about 50 at % for old NT100 is observed. However, the increase in oxygen content is even higher for oxygen plasma-treated NTs. In this case, about 57 at % of oxygen on the surface is observed. Interestingly, all oxygen plasma-treated NTs surfaces have practically the same chemical composition, and almost no fluorine is observed on the surface. After exposure to oxygen plasma, the carbon content is decreased to about 20 at %. The C/O and Ti/O ratios for each sample are presented in Table 1, together with wettability data and interaction of the surface with platelets.

A comparison of the XPS survey spectra for freshly prepared NTs with different nanotube diameters is presented in Figure 4. It can be clearly seen that the spectra for NTs with different

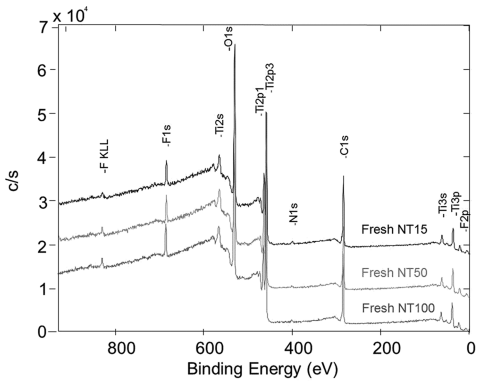

Figure 4. Comparison of XPS survey spectra on fresh nanotubes with 15, 50, and 100 nm in diameter (Fresh NT15, Fresh NT50, and Fresh NT100).

diameters does not differ much, and only a slight increase in the fluorine peak could be observed on NT50 and NT100, which is better seen in Figure 3 (chemical composition of the surface determined from the survey spectra).

In order to observe differences in chemical composition, high-resolution C 1s, O 1s, and Ti 2p were also recorded and compared. Not many differences in high-resolution peaks were observed between the samples, even in the case of freshly prepared, old, and plasma-treated NTs. Although higher oxygen and lower carbon contents were observed on plasma-treated surfaces, the high-resolution peaks were similar, indicating similar chemical groups to be present on the surface. For example, a comparison between the high-resolution peaks for freshly prepared and plasma-treated NT100 is presented in Figure 5. It can be observed that Ti 2p peaks are similar for both surfaces (fresh NT100 and NT100+P). The doublet peak at 458.7 and 464.5 eV for Ti 2p was observed, which is typical for the TiO_2 component. In the case of the high-resolution O 1s scan, the primary peak at a binding energy of 530.2 eV is observed, which is characteristic for Ti−O in the TiO_2 component. A minor subpeak at higher binding energies (about 531.7 eV) is also observed, especially in the case of fresh NT, which could correspond to OH on the surface of TiO_2.[36] It should be mentioned that a sharper O 1s peak is observed for the case of plasma-treated NTs, which could be correlated with a reduction in OH groups and a more stoichiometric oxide.[34] The high-resolution C 1s scan exhibits the main peak at 284.8 eV corresponding to C−C and C−H bonds and shoulder peaks appearing at 286.2 and 288.9 eV corresponding to C−O and C═O bonds, respectively. In the case of plasma-treated surface, the C 1s peak at 284.8 eV is broader (Figure 5).

2.3. Water Contact Angle Measurements. Water contact angle was measured on Ti foil and on TiO_2 NTs with different diameters. It was observed that freshly prepared TiO_2 NTs are hydrophilic with a water contact angle of less than 5 deg. However, the so-called aging of the surface[33] causing a wettability switch was observed for NTs after exposure to the atmosphere. In this case, surfaces become hydrophobic, with a contact angle of about 80 deg and more. After exposure of NTs to plasma, the switch in wettability is observed, and the surface again obtains its hydrophilic character, with a water contact angle of less than 5 deg.

2.4. Platelet Adhesion and Activation. The results of SEM analysis of whole blood interaction with Ti foil and nanotubes are presented in Figure 6. It can be observed that Ti foil promotes adhesion and activation of platelets as many spread and fully spread platelets can be seen on the surface (Figure 6a). They are already starting to aggregate and form fibrin structures, which could lead to undesired thrombus formation. Interestingly, tremendous differences in adhesion of platelets can be observed on NTs in regard to not only the NT diameter but also NT surface conditions (freshly fabricated, old, and plasma-treated). Differences in adhesion are already observed between fresh and old NTs (Figure 6b,c). Much lower platelet adhesion is observed on hydrophilic NTs (freshly prepared) compared to the hydrophobic NTs (aged). Interestingly, practically no platelets were observed on hydrophilic plasma-treated NTs. It is important to mention that according to XPS results, more oxygen was observed on these surfaces in comparison to freshly prepared NTs. The influence of the NT diameter on platelet adhesion was also observed. For example, on fresh NT15, many platelets in highly activated form (fully spread form) were observed, while only a few platelets in mostly round and dendritic form were observed on freshly prepared NT100. Adhesion and activation of platelets on old NTs surfaces were the highest for NT15 followed by NT50 and NT100 (Figure 6c). Images shown on Figure 6d present platelet adhesion on oxygen plasma-treated NTs. In this case, no significant influence of the NT diameter on adhesion of platelets was observed as a substantial decrease in platelet adhesion was observed practically on all plasma-treated surfaces. Practically, no platelets were observed on

https://dx.doi.org/10.1021/acsomega.9b04118
ACS Omega 2020, 5, 7280−7289

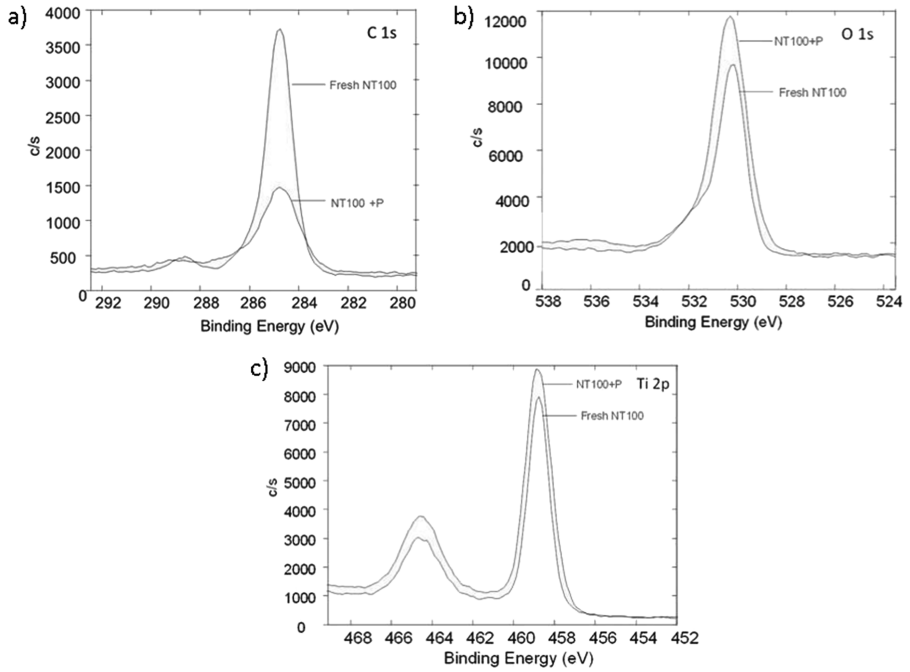

Figure 5. High-resolution (a) C 1s, (b) O 1s, and (c) Ti 2p peaks for fresh nanotubes with 100 nm in diameter (Fresh NT100) and plasma-treated nanotubes with 100 nm in diameter (NT100+P).

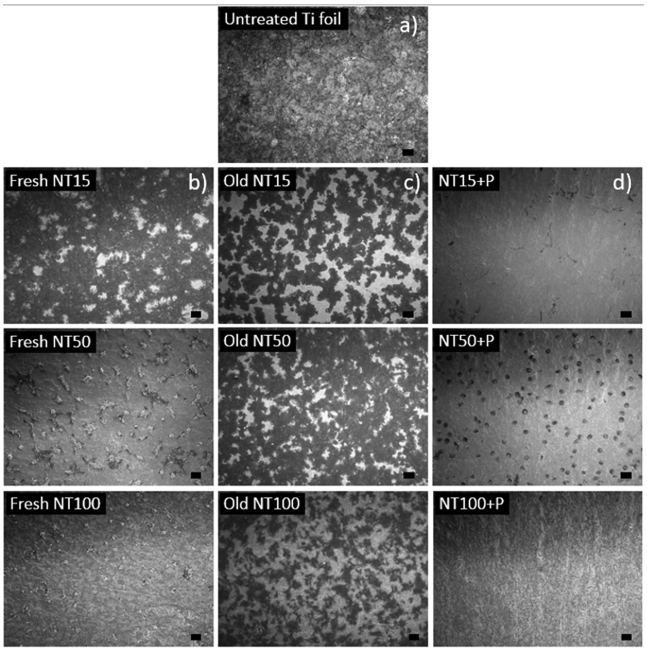

Figure 6. SEM images of (a) Ti foil, (b) fresh, (c) 2 months old, and (d) plasma-treated NT15, NT50, and NT100 interacting with platelets (NT: nanotubes with 15, 50, and 100 nm in diameter). Scale bars: 10 μm.

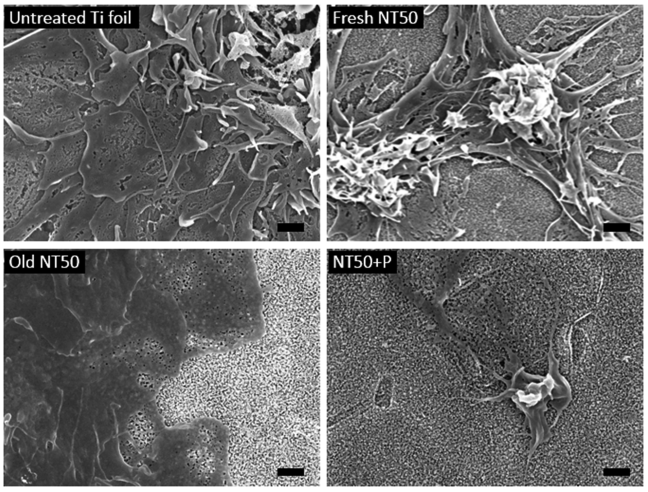

Figure 7. SEM images of Ti foil, fresh NT50, 1 month old NT50, and plasma-treated NT50 samples interacting with platelets (NT: nanotubes with 15, 50, and 100 nm in diameter). Ti foil: platelets numerous and fully spread, very high adhesion; Fresh NT50: platelets mainly in dendritic form, medium adhesion; Old NT50: platelets fully spread, high adhesion; NT50+P: platelets rounded and dendritic, low adhesion. Scale bars: 1 μm.

NT15 and NT100, while NT50 exhibited only a few, fully spread platelets, which were not aggregating. A comparison of SEM images at a higher magnification between Ti foil, fresh NT50, old NT50, and plasma-treated NT50 is shown in Figure 7. Platelets are well attached and spread on Ti foil, mainly in dendritic form. It can be seen that platelets spread mainly with filopodia on the fresh NT50 sample, while on the surface of old NT50, platelets are numerous and fully spread. On the contrary, the plasma-treated surface of NT50 inhibits the adhesion of platelets, which are mainly rounded or dendritic.

2.5. HCAEC Staining and Morphology. Images of HCAEC interactions with synthesized materials taken by fluorescence microscopy are shown in Figures 8 and 9. When HCAEC, which are not treated with acute-phase protein serum amyloid A (SAA), are grown on Ti foil, their phenotype represents that of control cells grown on plastic (Figure 8). Endothelial cells from human coronary arteries show distinct phenotypes after contact with increasing diameters of TiO_2 NTs. The smallest diameter of 15 nm provided for longitudinal growth and dynamic contact between cells, whereas upon

https://dx.doi.org/10.1021/acsomega.9b04118
ACS Omega 2020, 5, 7280−7289

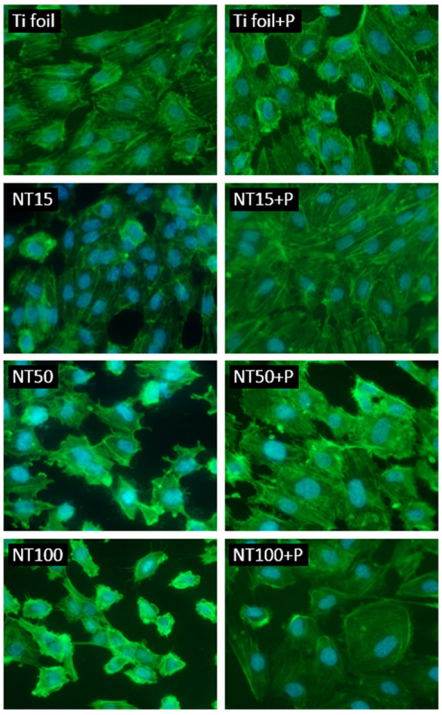

Figure 8. Fluorescence microscopy images of HCAEC grown on Ti foil, fresh NT15, fresh NT50, fresh NT100, plasma-treated NT15, plasma-treated NT50, and plasma-treated NT100 (NT: nanotubes with 15, 50, and 100 nm in diameter). Green is phalloidin-FITC staining, and blue is DAPI.

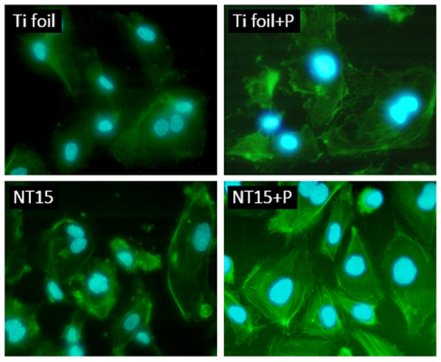

Figure 9. Fluorescence microscopy images of HCAEC grown on Ti foil, fresh NT15, and plasma-treated NT15 (NT: nanotubes with 15, 50, and 100 nm in diameter) for 2 days in the presence of SAA in medium in the last 24 h. Tests were conducted with acute-phase protein serum amyloid A (SAA). Green is phalloidin-FITC staining, and blue is DAPI.

adhesion and attachment to NTs with larger diameters, the cellular phenotypes changed, and a greater number of rounded cells emerged. The 100 nm NTs exhibited increasing stress, observed by the elevated number of blebbing cells. Plasma treatment on all NTs appears to recover "healthier" phenotypes of HCAEC, showing a smaller number of rounded cells on 50 nm NTs and less blebbing cells on the 100 nm NTs.

Due to the best performance of TiO_2 NTs with 15 nm in diameter in adhesion and proliferation of HCAEC, the experiments with the SAA (500 nM)-treated HCAEC were performed on this batch of samples, and the results are shown in Figure 9. In this case, fewer endothelial cells were found on the surface of Ti foil than in the experiment without SAA. Similar performance of endothelial cells was observed for the surface of TiO_2 NTs. However, plasma-treated TiO_2 NTs provided the optimal environment for attachment and growth of SAA-treated HCAEC.

2.6. HCASMC Staining and Morphology. As the adhesion and proliferation of HCAEC was the highest on TiO_2 NTs with 15 nm in diameter, the same experiments were performed on this batch of samples with vascular SMC. It can be seen from Figure 10, that smooth muscle cells that were not

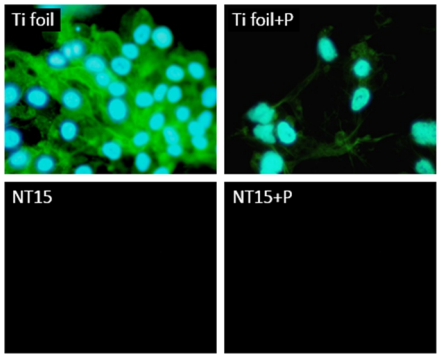

Figure 10. Fluorescence microscopy images of SMC grown on Ti foil, fresh NT15, and plasma-treated NT15 (NT: nanotubes with 15 nm in diameter) for 2 days.

treated with the acute phase protein SAA (500 nM) were readily attached to the surface of Ti foil in elongated form, with non-disrupted cytoplasm. Cells were found over the whole Ti foil surface. On the contrary, cells were not attached to the surface of NT15 and NT15 treated with oxygen plasma.

When SMC were treated with the acute phase protein SAA (500 nM) (Figure 11), the pro-inflammatory environment

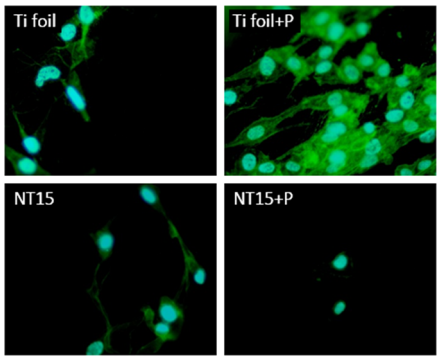

Figure 11. Fluorescence microscopy images of SMC grown on Ti foil, fresh NT15, and plasma-treated NT15 (NT: nanotubes with 15 nm in diameter) for 2 days. Tests were conducted with serum amyloid A (SAA 500 nM) addition in the cell culture media.

provided more optimal growth of SMC on the surface of NTs than without SAA. However, morphological changes of SMC were still observed; cells were extensively elongated or rounded on NT15 and NT15 treated with plasma, respectively, which suggests that these surfaces do not provide a sufficient environment for SMC adhesion and proliferation. This points to the fact that inflammation could drive SMC to adhere more readily to the NTs and indicates that the environment the cells are in is crucial for the success of the implants as well. It should

https://dx.doi.org/10.1021/acsomega.9b04118
ACS Omega 2020, 5, 7280−7289

be noted here that cells were attached only on the particular areas of the sample and did not cover the whole surface.

3. CONCLUSIONS

Platelet adhesion and activation on the surface of Ti materials were shown to depend on many factors: wettability, surface chemistry, morphology, and influence of the environment on cells (inflammation). Fresh NTs do not induce such intense platelet adhesion and activation as old NTs despite aging of the NTs causes switch of the hydrophilic surface to the hydrophobic, which is considered as less attractive for cell interactions. One of the reasons for better platelet adhesion and activation on the aged NTs could be higher oxygen concentration on the surface of the aged NTs. It was also shown that platelet adhesion and activation is greater on the surface of NTs with a lower diameter (15 nm) rather than on the surface of NTs with 100 nm in diameter. However, on plasma-treated surfaces, no platelets were observed, except few rounded platelets observed on NT50 samples. Plasma treatment has been shown to decrease blebbing of the human coronary artery endothelial cells and recovery of "healthier" phenotypes. Moreover, plasma treatment prevents the attachment and proliferation of smooth muscle cells on NTs with 15 nm in diameter, which is beneficial for vascular stent applications due to reduction of possible restenosis later on. Overall, plasma treatment of the NTs seems to act as a protective layer in keeping endothelial cells fit and growing while minimizing the number of smooth muscle cells and adhered and aggregated platelets. Moreover, plasma treatment also has a beneficial effect on cells growing in an inflammatory environment (in the presence of acute phase SAA), such as the reduction of SMC growth on NT15, which, to our knowledge, has never been shown before. Results of this study suggest that plasma-treated TiO_2 NTs could represent a new generation of vascular stents surfaces that would prevent clotting, thrombosis, and restenosis, which are still the major limitations of stent technology.

4. MATERIAL AND METHODS

4.1. Synthesis of TiO_2 Nanotubes. Titanium (Ti) foils (Advent, 0.1 mm in thickness, 99.6%) were used for preparation of different nanostructures. Prior to anodization, Ti foils were degreased by successive ultrasonication in acetone, ethanol, and deionized (DI) water for 5 min each and dried in a nitrogen stream. Nanorough surfaces were fabricated as per the method explained previously.[33] Briefly, ethylene glycol (Fluka, ≥99.5%)-based electrolytes containing specific concentrations of water and hydrofluoric acid (Sigma-Aldrich, ≥40%) were used to obtain different nanostructures, as shown in Table 2. All the anodization experiments were carried out at room temperature with platinum gauze as the counter electrode.

As-formed nanostructures were allowed to stand in ethanol for 2 h in order to remove organic components from the electrolyte solution. This step was followed by washing of the nanostructures with distilled water and drying under nitrogen stream.

4.2. Scanning Electron Microscopy (SEM). High-contrast images of TiO_2 NTs were obtained by scanning electron microscopy (Hitachi FE-SEM S4800). All samples were used without gold sputtering as formed samples already display images with reasonably good contrast.

Table 2. Anodization Conditions for Different Nanostructures (NT: Nanotubes)

sample	NT diameter (nm)	electrolyte	potential used (V)	anodization time (h)
NT15	15	EG + 8 M water + 0.2 M HF	10	2.5
NT50	50	EG + 8 M water + 0.2 M HF	20	2.5
NT100	100	EG + 8 M water + 0.2 M HF	58	2.5

4.3. Atomic Force Microscopy (AFM). Topographic features of TiO_2 NTs were examined by atomic force microscopy (Solver PRO, NT-MDT, Russia) in tapping mode in air. Samples were scanned with the standard Si cantilever with a force constant of 22 N/m and at a resonance frequency of 325 kHz (the tip radius was 10 nm, and the tip length was 95 μm). Average surface roughness (Ra) was measured from representative images on a 1×1 μm^2 area, and the scan rate was set at 1.3 Hz. The results are shown as the average Ra from five different areas.

4.4. Gaseous Plasma Treatment of Nanotubes. NTs were treated with oxygen plasma in the plasma reactor, evacuated with a two-stage oil rotary pump with a nominal pumping speed of 4.4×10^{-3} m^3/s. Plasma was created with an inductively coupled RF generator, operating at a frequency of 13.56 MHz and an output power of about 200 W. The system parameters were measured with a double Langmuir probe and a catalytic probe.[35,36] Commercially available oxygen was leaked into the discharge chamber Pyrex cylinder with a length of 0.6 m and an inner diameter of 0.036 m. The pressure was measured by an absolute vacuum gauge, and it was adjusted during continuous pumping by a precise leak valve. The pressure in our experiments was fixed at 75 Pa since, at this value, the highest degree of dissociation of gaseous molecules measured by the catalytic probes was detected. Plasma with an ion density of about 2×10^{15} m^{-3}, a thermal energy of 4 eV, and a neutral atom density of about 4×10^{21} m^{-3} was obtained at these discharge parameters. The NT samples placed on the glass holder were treated for 60s.

4.5. X-ray Photoelectron Spectroscopy (XPS). The X-ray photoelectron spectroscopy (XPS or ESCA) analyses were carried out on the PHI-TFA XPS spectrometer produced by Physical Electronics Inc. Samples were put on the sample holder and were introduced into the ultra-high vacuum spectrometer. The analyzed area was 0.4 mm in diameter, and the analyzed depth was about 3−5 nm. This high surface sensitivity is a general characteristic of the XPS method. Sample surfaces were excited by X-ray radiation from a monochromatic Al source at a photon energy of 1486.6 eV. The high-energy resolution spectra were acquired with an energy analyzer operating at a resolution of about 0.6 eV and a pass energy of 29 eV. During data processing, the spectra from the surface were aligned by setting the C 1s peak at 285.0 eV, characteristic for C−C bonds. The accuracy of binding energies was about ±0.3 eV. Quantification of surface composition was performed from XPS peak intensities taking into account relative sensitivity factors provided by the instrument manufacturer. Three different XPS measurements were performed on each sample, and average composition was calculated. The XPS spectra were measured on plain titanium and NTs (15, 50, and 100 nm in diameter) immediately after

https://dx.doi.org/10.1021/acsomega.9b04118
ACS Omega 2020, 5, 7280−7289

the anodization procedure (fresh NT), after 1 month aging at room temperature (old NT), and immediately after plasma treatment (NT+P).

4.6. Water Contact Angle Measurements. The surface wettability was measured 1 week after NTs were produced by anodization, after 1 month of aging at room temperature, and immediately after NTs were treated by oxygen plasma. A demineralized water droplet of 3 μL volume was put on the surface and measured with a home-made apparatus equipped with a CCD camera and a PC computer, which enables high-resolution micrographs of a water drop on the sample surface. For each sample, 10 measurements were performed in order to minimize statistical error. The relative humidity was kept at 45% and the temperature at 22 °C. The contact angles were determined by our own software, which enabled fitting of the water drop on the surface in order to allow for a relatively precise determination of the contact angle.

4.7. Incubation with Whole Blood. Whole blood was obtained from healthy volunteers via vein puncture. The blood was drawn into 9 mL tubes coated with trisodium citrate anticoagulant (Sigma-Aldrich). The number of platelets in whole blood was counted with a multi-parameter automated hematology analyzer (Cell-DYN 3200, Abbott). The material samples, plain Ti foil and fresh, old, and plasma-treated NTs with different diameters (NT15, NT50, and NT100) with 10 mm × 10 mm in size, were incubated with 1 mL of whole blood for 1 h at room temperature with gentle shaking at 300 rpm in the 24-well cell culture plates. Afterward, 1 mL of PBS (phosphate-buffered saline) was added to the incubated samples. The blood with PBS was then removed, and the samples were rinsed five times with 2 mL of PBS in order to remove weakly adherent platelets. The test was done in triplicate, and the representative images are shown.

4.8. Preparation of Samples for SEM Analysis. The preparation of the TiO_2 NTs and Ti foil samples for SEM analysis was performed in the following manner: The samples, prepared as described in section 4.7, were dipped within 400 μL of 1% paraformaldehyde (PFA) solution for 15 min at room temperature. Then, the materials were rinsed with PBS and dehydrated by using a graded ethanol series (50, 70, 80, 90, 100, and again 100 vol % of ethanol) for 5 min and, in the last stage, in the series (100 vol % ethanol) for 15 min. Afterward, the samples were dried with a Critical Point Dryer and as-such coated with gold and examined by means of SEM (Carl Zeiss Supra 35 VP) at an accelerating voltage of 1 keV.

4.9. Cell Culture. Human coronary artery endothelial cells (HCAEC) were purchased from Lifeline Cell Technology (Frederick, MD, USA), and human coronary artery smooth muscle cells (HCASMC) were purchased from ProVitro AG (Berlin, Germany). HCAEC and HCASMC were plated into 75 cm^2 flasks (TPP, Trasadigen, Switzerland) at 37 °C in a humidified atmosphere at 5% CO_2 and grown in a VascuLife EnGS endothelial medium complete kit (Frederick, MD, USA) and Smooth muscle cell growth medium FCS-kit (ProVitro AG, Berlin, Germany), respectively, following manufacturer's instructions. For experiments, sub-confluent cell cultures were used between passages 4 and 6.

4.10. Immunofluorescence Microscopy and Cell Morphology. HCAEC and SMC were seeded onto foil and NTs of different pore size diameters (15, 50, and 100 nm) and foil and 15 nm NTs, respectively. The cells on sample materials were placed into 12-well plates at a density of 20 × 10^3 cells per cm^2 and grown for 2 days, and the test was conducted in triplicate. In indicated cases, SAA (final concentration of 500 nM) was added into cell media 24 h before staining. Staining with fluorescein phalloidin (Molecular Probes, Thermo Fisher Scientific) was performed following manufacturer's instructions. Briefly, cells were washed two times for 3 min with PBS, pH 7.4, fixed in 3.7% formaldehyde solution for 10 min, and washed three times for 3 min with PBS at room temperature. Cells were incubated in detergent 0.1% Triton X-100 for 4 min and then washed with PBS three times for 3 min. Dye stock was diluted (1:40) in PBS with 1% BSA and applied to HCAEC and SMC for 30 min. Final washing steps were performed three times for 3 min with PBS. DAPI (4′,6-diamidino-2-phenylindole) staining (Molecular Probes, Thermo Fisher Scientific) was performed following manufacturer's instructions. Briefly, samples were incubated with 300 nM DAPI in PBS for 5 min and washed with PBS for 3 min at room temperature. SlowFade reagent (Thermo Fisher Scientific, USA) was applied to HCAEC and SMC (one drop), and a cover slip was fixed on top with clear nail polish. Slides were examined and/or stored in the dark at 4 °C. Images were generated using the fluorescence microscope Nikon eclipse E400 and a digital camera (Nikon Instruments, Dusseldorf, Germany). Analysis was performed with Nikon ACT-1 imaging software, and the representative images are presented.

AUTHOR INFORMATION

Corresponding Author

Ita Junkar − *Department of Surface Engineering and Optoelectronics, Jožef Stefan Institute, SI-1000 Ljubljana, Slovenia*; Phone: +38614473885; Email: ita.junkar@ijs.si

Authors

Mukta Kulkarni − *Laboratory of Biophysics, Faculty of Electrical Engineering, University of Ljubljana, SI-1000 Ljubljana, Slovenia*

Metka Benčina − *Department of Surface Engineering and Optoelectronics, Jožef Stefan Institute, SI-1000 Ljubljana, Slovenia*; orcid.org/0000-0002-6431-6544

Janez Kovač − *Department of Surface Engineering and Optoelectronics, Jožef Stefan Institute, SI-1000 Ljubljana, Slovenia*

Katjuša Mrak-Poljšak − *Department of Rheumatology, University Medical Centre Ljubljana, SI-1000 Ljubljana, Slovenia*

Katja Lakota − *Department of Rheumatology, University Medical Centre Ljubljana, SI-1000 Ljubljana, Slovenia*

Snežna Sodin-Šemrl − *Department of Rheumatology, University Medical Centre Ljubljana, SI-1000 Ljubljana, Slovenia*

Miran Mozetič − *Department of Surface Engineering and Optoelectronics, Jožef Stefan Institute, SI-1000 Ljubljana, Slovenia*

Aleš Iglič − *Laboratory of Biophysics, Faculty of Electrical Engineering and Faculty of Medicine, University of Ljubljana, SI-1000 Ljubljana, Slovenia*

Complete contact information is available at: https://pubs.acs.org/10.1021/acsomega.9b04118

Notes

The authors declare no competing financial interest.

https://dx.doi.org/10.1021/acsomega.9b04118
ACS Omega 2020, 5, 7280−7289

■ ACKNOWLEDGMENTS

The authors would like to acknowledge the Slovenian Research Agency for financial support (grants nos. L7-7566, P2-0232, and P3-0314) and Slovenian Ministry of Education, Science and Sport grant "Public call for encouraging young investigators at the beginning of their career 2.0" (no. 5442-15/2016/18). The authors also acknowledge the use of equipment in the Center of Excellence on Nanoscience and Nanotechnology - Nanocenter at Jozef Stefan Institute, Ljubljana SI-1000, Slovenia.

■ REFERENCES

(1) Chaabane, C.; Otsuka, F.; Virmani, R.; Bochaton-Piallat, M. L. Biological responses in stented arteries. *Cardiovasc. Res.* **2013**, *99*, 353−363.

(2) Dangas, G. D.; Schoos, M. M.; Steg, P. G.; Mehran, R.; Clemmensen, P.; van't Hof, A.; Prats, J.; Bernstein, D.; Deliargyris, E. N.; Stone, G. W. Early Stent Thrombosis and Mortality After Primary Percutaneous Coronary Intervention in ST-Segment-Elevation Myocardial Infarction A Patient-Level Analysis of 2 Randomized Trials. *Circ.: Cardiovasc. Interventions* **2016**, *9*, 15.

(3) Serebruany, V. L.; Cherepanov, V.; Golukhova, E. Z.; Kim, M. H. The Dual Antiplatelet Therapy Trial after the FDA Update: Noncardiovascular Deaths Cancer and Optimal Treatment Duration. *Cardiology.* **2015**, *132*, 74−80.

(4) Acharya, G.; Park, K. Mechanisms of controlled drug release from drug-eluting stents. *Adv. Drug Delivery Rev.* **2006**, *58*, 387−401.

(5) Costa, R. A.; Sousa, J. E.; Abizaid, A.; Chaves, A.; Feres, F.; Sousa, A. G. M. R.; Musumeci, G.; Mehran, R.; Fitzgerald, P. J.; Lansky, A. J.; Leon, M. B.; Shiran, A.; Halon, D. A.; Lewis, B. S.; Guagliumi, G. The randomised study of the double dose versus single dose sirolimus-eluting stent for the treatment of diabetic patients with de novo coronary lesions. *EuroIntervention : J. EuroPCR Collab. Work. Group Interventional Cardiol. Eur. Soc. Cardiol.* **2006**, *2*, 295−301.

(6) Lewis, A. L.; Tolhurst, L. A.; Stratford, P. W. Analysis of a phosphorylcholine-based polymer coating on a coronary stent pre- and post-implantation. *Biomaterials* **2002**, *23*, 1697−1706.

(7) Jordan, S. W.; Chaikof, E. L. Novel thromboresistant materials. *J. Vasc. Surg.* **2007**, *45*, 104−115.

(8) Malik, S. M.; Mukherjee, A. Implantable medical device i.e. stent, for treating blood vessel occlusions, has titanium nitride carbide compound implanted at predetermined depth within region of tissue-contacting surface. US2,013172,974-A1; US8,834,555-B2; US2,013,172,974-A1 04 Jul 2013 A61F-002/82 201346.

(9) Ozaltin, K.; Lehocký, M.; Kuceková, Z.; Humpolíček, P.; Sáha, P. A novel multistep method for chondroitin sulphate immobilization and its interaction with fibroblast cells. *Mater. Sci. Eng. C.* **2017**, *70*, 94−100.

(10) Kulkarni, M.; Mazare, A.; Gongadze, E.; Perutkova, Š.; Kralj-Iglič, V.; Milošev, I.; Schmuki, P.; Iglič, A.; Mozetič, M. Titanium nanostructures for biomedical applications. *Nanotechnology* **2015**, *26*, No. 062002.

(11) Kulkarni, M.; Mazare, A.; Schmuki, P.; Iglič, A. Biomaterial surface modification of titanium and titanium alloys for medical applications. *Nanomedicine* **2014**, *111*, 111.

(12) Mohan, C. C.; Chennazhi, K. P.; Menon, D. In vitro hemocompatibility and vascular endothelial cell functionality on titania nanostructures under static and dynamic conditions for improved coronary stenting applications. *Acta Biomater.* **2013**, *9*, 9568−9577.

(13) Dalby, M. J.; Riehle, M. O.; Johnstone, H.; Affrossman, S.; Curtis, A. S. G. In vitro reaction of endothelial cells to polymer demixed nanotopography. *Biomaterials* **2002**, *23*, 2945−2954.

(14) Das, K.; Bose, S.; Bandyopadhyay, A. TiO_2 nanotubes on Ti: Influence of nanoscale morphology on bone cell-materials interaction. *J. Biomed. Mater. Res., Part A* **2009**, *90*, 225−237.

(15) Kulkarni, M.; Flašker, A.; Lokar, M.; Mrak-Poljšak, K.; Mazare, A.; Artenjak, A.; Čučnik, S.; Kralj, S.; Velikonja, A.; Schmuki, P.; Kralj-Iglič, V.; Sodin-Semrl, S.; Iglič, A. Binding of plasma proteins to titanium dioxide nanotubes with different diameters. *Int. J. Nanomed.* **2015**, *10*, 1359−1373.

(16) Park, J.; Bauer, S.; Schlegel, K. A.; Neukam, F. W.; von der Mark, K.; Schmuki, P. TiO_2 Nanotube Surfaces: 15 nm - An Optimal Length Scale of Surface Topography for Cell Adhesion and Differentiation. *Small* **2009**, *5*, 666−671.

(17) Ai, S.; He, Q.; Tian, Y.; Li, J. Fabrication of mesoporous titanium oxide nanotubes based on layer-by-layer assembly. *J. Nanosci. Nanotechnol.* **2007**, *7*, 2534−2537.

(18) Wei, D.; Feng, W.; Du, Q.; Zhou, R.; Li, B.; Wang, Y.; Zhou, Y.; Jia, D. Titania nanotube/nano-brushite composited bioactive coating with micro/nanotopography on titanium formed by anodic oxidation and hydrothermal treatment. *Ceram. Int.* **2015**, *41*, 13115−13125.

(19) Lorenzetti, M.; Pellicer, E.; Sort, J.; Baró, M. D.; Kovač, J.; Novak, S.; Kobe, S. Improvement to the Corrosion Resistance of Ti-Based Implants Using Hydrothermally Synthesized Nanostructured Anatase Coatings. *Materials.* **2014**, *7*, 180−194.

(20) Zwilling, V.; Aucouturier, M.; Darque-Ceretti, E. Anodic oxidation of titanium and TA6V alloy in chromic media. An electrochemical approach. *Electrochim Acta.* **1999**, *45*, 921−929.

(21) Macak, J. M.; Tsuchiya, H.; Berger, S.; Bauer, S.; Fujimoto, S.; Schmuki, P. On wafer TiO_2 nanotube-layer formation by anodization of Ti-films on Si. *Chem. Phys. Lett.* **2006**, *428*, 421−425.

(22) Albu, S. P.; Ghicov, A.; Aldabergenova, S.; Drechsel, P.; LeClere, D.; Thompson, G. E.; Macak, J. M.; Schmuki, P. Formation of Double-Walled TiO2 Nanotubes and Robust Anatase Membranes. *Adv. Mater* **2008**, *20*, 4135.

(23) Kulkarni, M.; Mazare, A.; Park, J.; Gongadze, E.; Killian, M. S.; Kralj, S.; von der Mark, K.; Iglič, A.; Schmuki, P. Protein interactions with layers of TiO_2 nanotube and nanopore arrays: Morphology and surface charge influence. *Acta Biomater.* **2016**, *45*, 357−366.

(24) Puckett, S.; Pareta, R.; Webster, T. J. Nano rough micron patterned titanium for directing osteoblast morphology and adhesion. *Int. J. Nanomedicine.* **2008**, *3*, 229−241.

(25) Bjursten, L. M.; Rasmusson, L.; Oh, S.; Smith, G. C.; Brammer, K. S.; Jin, S. Titanium dioxide nanotubes enhance bone bondingin vivo. *J. Biomed. Mater. Res.* **2009**, *9999A*, 1218−1224.

(26) Ding, X. L.; Zhou, L.; Wang, J.; Zhao, Q.; Lin, X.; Gao, Y.; Li, S.; Wu, J.; Rong, M.; Guo, Z.; Lai, C.; Lu, H.; Jia, F. The effects of hierarchical micro/nanosurfaces decorated with TiO_2 nanotubes on the bioactivity of titanium implants in vitro and in vivo. *Int. J. Nanomedicine.* **2015**, *10*, 6955−6973.

(27) Neacsu, P.; Mazare, A.; Schmuki, P.; Cimpean, A. Attenuation of the macrophage inflammatory activity by TiO_2 nanotubes via inhibition of MAPK and NF-κB pathways. *Int. J. Nanomed.* **2015**, *10*, 6455−6467.

(28) Smith, B. S.; Yoriya, S.; Grissom, L.; Grimes, C. A.; Popat, K. C. Hemocompatibility of titania nanotube arrays. *J. Biomed. Mater. Res.* **2010**, *95A*, 350−360.

(29) Yang, Y.; Lai, Y.; Zhang, Q.; Wu, K.; Zhang, L.; Lin, C.; Tang, P. A novel electrochemical strategy for improving blood compatibility of titanium-based biomaterials. *Colloids Surf., B* **2010**, *79*, 309−313.

(30) Flašker, A.; Kulkarni, M.; Mrak-Poljšak, K.; Junkar, I.; Čučnik, S.; Žigon, P.; Mazare, A.; Schmuki, P.; Iglič, A.; Sodin-Semrl, S. Binding of Human Coronary Artery Endothelial Cells to Plasma-treated Titanium Dioxide Nanotubes of Different Diameters. *J. Biomed. Mater. Res., Part A* **2016**, 1113.

(31) Huang, N.; Yang, P.; Leng, Y. X.; Chen, J. Y.; Sun, H.; Wang, J.; Wang, G. J.; Ding, P. D.; Xi, T. F.; Leng, Y. Hemocompatibility of titanium oxide films. *Biomaterials* **2003**, *24*, 2177−2187.

(32) Riedel, N. A.; Smith, B. S.; Williams, J. D.; Popat, K. C. Improved thrombogenicity on oxygen etched Ti6Al4V surfaces. *Mater. Sci. Eng. C.* **2012**, *32*, 1196−1203.

(33) Kulkarni, M.; Patil-Sen, Y.; Junkar, I.; Kulkarni, C. V.; Lorenzetti, M.; Iglič, A. Wettability studies of topologically distinct titanium surfaces. *Colloids Surf., B* **2015**, *129*, 47−53.

https://dx.doi.org/10.1021/acsomega.9b04118
ACS Omega 2020, 5, 7280−7289

(34) Canal, C.; Gaboriau, F.; Ricard, A.; Mozetic, M.; Cvelbar, U.; Drenik, A. Density of O-atoms in an Afterglow Reactor During Treatment of Wool. *Plasma Chem. Plasma Process.* **2007**, *27*, 404−413.
(35) Poberaj, I.; Mozetič, M.; Babič, D. Comparison of fiber optics and standard nickel catalytic probes for determination of neutral oxygen atoms concentration. *J. Vac. Sci. Technol., A* **2002**, *20*, 189−193.
(36) Healy, K. E.; Ducheyne, P. THE MECHANISMS OF PASSIVE DISSOLUTION OF TITANIUM IN A MODEL PHYSIOLOGICAL ENVIRONMENT. *J. Biomed. Mater. Res.* **1992**, *26*, 319−338.

https://dx.doi.org/10.1021/acsomega.9b04118
ACS Omega 2020, 5, 7280−7289